

Strong coupling of virtual negative states in the Kapitza-Dirac effect

Qianlong Wang,¹ Sven Ahrens,^{1,*} and Baifei Shen^{1,†}

¹*Department of Physics, Shanghai Normal University, Shanghai 200234, China*

(Dated: January 13, 2026)

Negative states are an intrinsic property of relativistic quantum theory and related to anti-particles in the context of the Dirac sea concept. We show that negative states can dominantly contribute to the diffraction amplitude in the quantum dynamics of the two-photon Kapitza-Dirac effect. We draw our conclusion by investigating solutions from time-dependent perturbation theory, where the perturbative solutions are in match with numeric solutions of the relativistic quantum system and also with the numeric and analytic solutions from the relativistic equations of motion of a classical point-like electron in an external standing wave light field. While our numeric solutions assume a strong laser field, the analytic solutions indicate that negative state coupling remains dominant for arbitrary low field amplitudes, where in the single-photon case (Compton scattering) negative state coupling can be mathematically associated with the interaction of a virtual electron-positron pair in the context of a quantized theory in old-fashioned perturbation theory.

I. INTRODUCTION

Negative solutions arise naturally in relativistic single particle quantum theory, due to quadratic energy and momentum components in the relativistic energy-momentum relation and thus imply corresponding positive and negative energy eigenstates in the quantum system. Accordingly, the Klein-Gordon and Dirac equations are known to have solutions with negative energy eigenvalues [1–6], which gave a theoretical indication for the existence of positrons [7, 8]. This paradoxical situation is handled by adding up negative solutions with their positive absolute value of the energy eigenvalue in the Hamiltonian, when quantizing the fields [9–11]. Nevertheless, it is possible to associate negative states of a single-particle theory with virtual excitations of pairs (of particle and anti-particle) in the context of such a quantized interacting theory, for the case of Compton scattering [12].

An interesting aspect in this context is the circumstance that the lower two components of the Dirac equation are reinserted into the upper two components, when deducing the non-relativistic limit of the Dirac equation [1–3]. The result of this non-relativistic limit procedure yields the well-known $(\mathbf{p} - e\mathbf{A}/c)^2$ expression in the Schrödinger equation, which is the reason for us to provide a summary of its commonly known derivation in appendix A. The mentioned upper and lower components, in turn, can approximately be associated with the positive and negative bi-spinor solutions of the Dirac equation for the case of non-relativistic momenta $|\mathbf{p}| \ll mc$. Therefore the question arises: How strong are those negative states actually coupled in the quantum dynamical evolution of an interacting theory with non-vanishing external fields $\mathbf{A} \neq 0$?

In this article, we investigate the coupling of negative states for the case of the Kapitza-Dirac effect [13–

15], in which the electron is interacting with a standing wave of light. A common method [12, 16–18] for numerically and analytically describing the quantum dynamics in terms of the energy-eigenstates allows a precise tracking of the coupling strength of negative states, in the framework of time-dependent perturbation theory. The circumstance that a precise experimental implementation of the Kapitza-Dirac effect already exists [19, 20], and the mentioned association of negative states with virtual anti-particle excitations [12] matches the Kapitza-Dirac effect, emphasizes the significance of this study.

Our article is structured as follows: The relativistic quantum framework is introduced in Section II, where we first introduce the optical standing light wave in section II A. We then introduce the equations of motion (Dirac equation) for the relativistic quantum dynamics of the electron in section II B, which are subsequently solved numerically in section II C for the 2-photon Kapitza-Dirac effect. A perturbative analysis of the process follows in section II D, which allows us to study the coupling to negative states in Section II E. We conclude the investigation of the relativistic electron quantum dynamics by performing an approximation of the perturbative solution for small transverse electron momenta in section II F. Transitioning to the non-relativistic quantum description, Section III discusses the Schrödinger equation for modeling the electron quantum dynamics (Section III A), with corresponding perturbative solutions derived in Section III B. Section IV introduces a non-relativistic classical treatment by deriving the ponderomotive potential, where the classical interaction with the field can be linked to the quantum processes. In Section V we extend this framework towards the classical relativistic equations of motion and demonstrate a match with the relativistic quantum solution. We finally discuss the role of negative states in quantum dynamics and their relation to the classical motion in section VI and conclude with an outlook to related questions of our findings in section VII.

* ahrens@shnu.edu.cn

† bfshen@shnu.edu.cn

II. RELATIVISTIC QUANTUM DESCRIPTION

A. Laser setup

The setup of consideration in this article is the 2-photon Kapitza-Dirac effect, in which an electron is diffracted in a standing wave of light, given by the vector potential [16, 17]

$$\mathbf{A}(\mathbf{x}, t) = \mathbf{A}_0 \cos(\mathbf{k} \cdot \mathbf{x}) \sin(\omega t) \xi(t). \quad (1)$$

Here, we introduce the laser wave vector $\mathbf{k} = (k_L, 0, 0)$, the laser frequency $\omega = ck_L$ and a temporal envelope function

$$\xi(t) = \begin{cases} \sin^2(\frac{\pi t}{2\Delta T}) & \text{if } 0 \leq t \leq \Delta T, \\ 1 & \text{if } \Delta T \leq t \leq T - \Delta T, \\ \sin^2(\frac{\pi(T-t)}{2\Delta T}) & \text{if } T - \Delta T \leq t \leq T, \\ 0 & \text{else,} \end{cases} \quad (2)$$

for modeling the turn on and turn off of the standing light wave. In the envelope function, we also denote the turn on and turn off time ΔT and total interaction time T . We further mention, that we are working in a Gaussian unit system for all calculations in this article, with the vacuum speed of light c , the electron mass m , the elementary charge e and the reduced Planck constant \hbar . The polarization and amplitude of the standing light wave is parameterized by the vector $\mathbf{A}_0 = (0, 0, A_0)$, which is pointing along the \mathbf{e}_3 direction.

B. Dirac equation

We start our investigation of the coupling to negative states with the relativistic quantum description for spin 1/2 particles, which is formulated in terms of the Dirac equation. We will later draw an analogy to non-relativistic quantum dynamics in terms of the Schrödinger equation and after that further consider the relation to classical mechanics.

We denote the Dirac equation by

$$i\hbar \dot{\Psi}(\mathbf{x}, t) = H\Psi(\mathbf{x}, t) \quad (3)$$

with the Dirac Hamiltonian [1, 2]

$$H = c\boldsymbol{\alpha} \left(\mathbf{p} - \frac{e}{c} \mathbf{A} \right) + \beta mc^2, \quad (4)$$

which we couple to the vector potential in Eq. (1) only, in this article. The 4×4 matrices $\boldsymbol{\alpha} = (\alpha_1, \alpha_2, \alpha_3)^T$ and β are

$$\boldsymbol{\alpha}_i = \begin{pmatrix} 0 & \sigma_i \\ \sigma_i & 0 \end{pmatrix}, \quad \beta = \begin{pmatrix} \mathbf{1} & 0 \\ 0 & -\mathbf{1} \end{pmatrix}, \quad (5)$$

with the 2×2 identity $\mathbf{1}$ and the Pauli matrices σ_i . The Dirac Hamiltonian (4) can be decomposed into a free

Hamiltonian H_0 and an interaction part V

$$H_0 = c\boldsymbol{\alpha} \cdot \mathbf{p} + \beta mc^2 \quad (6a)$$

$$V = -e\boldsymbol{\alpha} \cdot \mathbf{A}. \quad (6b)$$

Furthermore, in analogy to previous investigations [12, 16–18], the Dirac wave function $\Psi(\mathbf{x}, t)$ is expanded into plane waves

$$\Psi(\mathbf{x}, t) = \sum_{n, \gamma, s} c_n^{\gamma, s}(t) \psi_n^{\gamma, s}(\mathbf{x}) \quad (7)$$

with basis elements

$$\psi_n^{\gamma, s}(\mathbf{x}) = \sqrt{\frac{k_L}{2\pi}} u_n^{\gamma, s} e^{i\mathbf{p}_n \cdot \mathbf{x}}, \quad (8)$$

electron polarizations $\gamma \in \{+, -\}$, spin polarizations $s \in \{\uparrow, \downarrow\}$ and discrete momenta $\mathbf{p}_n = \mathbf{p}_0 + n\hbar\mathbf{k}_L$. The number n represents the number of laser photon momenta along the laser propagation direction in momentum space and the complex amplitudes $c_n^{\gamma, s}(t)$ serve as expansion coefficients for $\Psi(\mathbf{x}, t)$ with respect to the basis functions $\psi_n^{\gamma, s}(\mathbf{x})$. The explicit form of the bi-spinors $u_n^{\gamma, s} = u^{\gamma, s}(\mathbf{p}_n)$ is given by

$$u^{+, s}(\mathbf{p}) = \sqrt{\frac{\mathcal{E}_n + mc^2}{2\mathcal{E}_n}} \begin{pmatrix} \chi^s \\ \frac{\boldsymbol{\sigma} \cdot \mathbf{cp}}{\mathcal{E}_n + mc^2} \chi^s \end{pmatrix} \quad (9a)$$

and

$$u^{-, s}(\mathbf{p}) = \sqrt{\frac{\mathcal{E}_n + mc^2}{2\mathcal{E}_n}} \begin{pmatrix} -\frac{\boldsymbol{\sigma} \cdot \mathbf{cp}}{\mathcal{E}_n + mc^2} \chi^s \\ \chi^s \end{pmatrix} \quad (9b)$$

with the two spin polarizations

$$\chi^\uparrow = \begin{pmatrix} 1 \\ 0 \end{pmatrix} \quad \chi^\downarrow = \begin{pmatrix} 0 \\ 1 \end{pmatrix}. \quad (10)$$

We also point out that the basis functions $\psi_n^{\gamma, s}(\mathbf{x})$ are eigenfunctions of the free, time-independent Dirac Hamiltonian H_0 with energy eigenvalue

$$\mathcal{E}_n = \sqrt{mc^2 + \mathbf{p}_n^2 c^2} \quad (11)$$

and frequencies $\omega_n = \mathcal{E}_n/\hbar$.

C. Numerical solution

An equation of motion for the expansion coefficients $c_n^{\gamma, s}(t)$ can be obtained by inserting the wave function expansion (7) into the Dirac equation (3) and projecting with the basis functions (8) from the left. The projection operation can be implemented by integration over one wave length $\lambda = 2\pi/k_L$ along the laser direction, resulting in the momentum space notion for the Dirac equation [16, 17, 21]

$$i\hbar \dot{c}_n^{\gamma, s}(t) = \pm \mathcal{E}_n c_n^{\gamma, s}(t) + \sum_{n', \gamma', s'} V_{n, n'}^{\gamma, s; \gamma', s'}(t) c_{n'}^{\gamma', s'}(t). \quad (12)$$

At this point we have introduced the interaction matrix elements in the Schrödinger picture

$$\begin{aligned}
& V_{n,n'}^{\gamma,s;\gamma',s'}(t) \\
&= \frac{1}{\lambda} \int_{-\lambda/2}^{\lambda/2} dx [\psi_n^{\gamma,s}(\mathbf{x})]^\dagger [-e\boldsymbol{\alpha} \cdot \mathbf{A}(\mathbf{x},t)] \psi_{n'}^{\gamma',s'}(\mathbf{x}) \\
&= -\frac{eA_0 \sin(\omega t) \xi(t)}{2} L_{n,n'}^{\gamma,s;\gamma',s'} \delta_{n,n'+1} \\
&\quad - \frac{eA_0 \sin(\omega t) \xi(t)}{2} L_{n,n'}^{\gamma,s;\gamma',s'} \delta_{n,n'-1}
\end{aligned} \tag{13}$$

and the spinor-matrix elements

$$L_{n,n'}^{\gamma,s;\gamma',s'} = \left[(u_n^{\gamma,s})^\dagger \alpha_3 (u_{n'}^{\gamma',s'}) \right]. \tag{14}$$

The equation of motion in momentum space (12) allows for studying the influence of negative state coupling on the quantum dynamics of the electron, by toggling the interactions $V_{n,n'}^{\pm,s;\mp,s'}$ on and off. We illustrate this for the case of a numerical solution of Eq. (12), which is displayed in Fig. 1(a), where we set the laser frequency $\omega = ck_L = 0.02 mc^2/\hbar$, the electron initial momentum $\mathbf{p}_0 = (-\hbar k_L, 0, 0)$ and the initial quantum state

$$c_0^{+,\uparrow}(0) = 1, \quad c_n^{\gamma,s}(0) = 0, \text{ else.} \tag{15}$$

The quantum state is evolved in the external standing wave laser field (1) parameterized by a turn-on and turn-off time of ten laser periods $\Delta T = 5 \times 2\pi/\omega$, with the laser field amplitude $eA_0 = 0.01 mc^2$. We observe in Fig. 1(a) sinusoidally oscillating occupation probabilities, which are consistent with the literature [14, 15], and which are termed Rabi oscillations [22].

When redoing the simulation with the matrix entries $V_{n,n'}^{\pm,s;\pm,s'}$ set to zero, we obtain dynamics which appear to be identical to the Rabi oscillations as shown in Fig. 1(a). Oppositely, we observe a drastic change of the dynamics when setting only the matrix entries $V_{n,n'}^{\pm,s;\mp,s'}$ to zero in Eq. (12), as shown in Figs. 1(b) and 1(c). We see in Figs. 1(b) and 1(c) the beginning of Rabi cycles with a Rabi period which is orders of magnitudes larger than the Rabi oscillation period in Fig. 1(a). Therefore, we are led to the conclusion that the couplings between negative and positive states $V_{n,n'}^{\pm,s;\mp,s'}$ contribute significantly more to the quantum dynamics than the couplings $V_{n,n'}^{\pm,s;\pm,s'}$, which only mediate within the positive and negative spectrum.

In order to further identify characteristic features of the diffraction probability in a later comparison with perturbative results, we display the momentum dependence of the resulting diffraction probability

$$|c_2^+(t)|^2 = |c_2^{+,\uparrow}(t)|^2 + |c_2^{+,\downarrow}(t)|^2 \tag{16}$$

for multiple simulations with different momenta p_3 in the initial momentum $\mathbf{p}_0 = (-\hbar k_L, 0, p_3)$ at time $T = 150 \times 2\pi/\omega$ in Fig. 2.

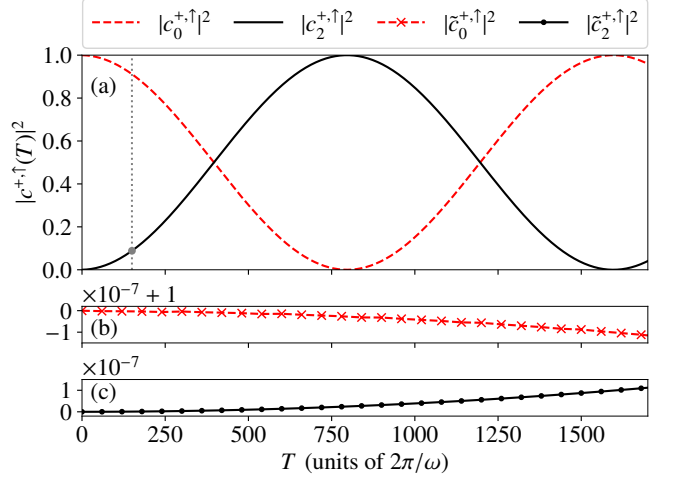


FIG. 1. Occupation probabilities as a function of the full interaction time T for the dynamics of the simulated two-photon Kapitza-Dirac effect. (a) Displayed are the absolute value squares of the only non-vanishing expansion coefficients $c_0^{+,\uparrow}$ and $c_2^{+,\uparrow}$ for a simulation of the equation of motion (12) with initial condition (15) and parameters $k_L = 0.02 mc/\hbar$, $\Delta T = 5 \times 2\pi/\omega$ and $eA_0 = 0.01 mc^2$. The observed Rabi period of 1600 laser cycles can be deduced analytically, as done in Eq. (54) by a calculation using time dependent perturbation theory. The gray dotted line marks the simulation time at which the diffraction probability as a function of the transverse momentum p_3 is displayed in Fig. 2. Panels (b) and (c) show the quantities $|c_0^{+,\uparrow}|^2$ and $|c_2^{+,\uparrow}|^2$, respectively, for which the simulation in panel (a) is redone with the matrix entries $V_{n,n'}^{\pm,s;\mp,s'}$ set to zero.

D. Perturbative solution

For a more detailed study of the contribution of negative energy eigenstates in the quantum dynamics as shown in Figs. 1 and 2, we are now discussing the perturbative short-time solution for the description of the process here, by following the conventions in references [12, 17, 21, 23]. The diffraction amplitude of the two-photon Kapitza-Dirac effect can be encoded by the time-evolution of the two-component object

$$c_n^+(t) = \begin{bmatrix} c_n^{+,\uparrow}(t) \\ c_n^{+,\downarrow}(t) \end{bmatrix}, \tag{17}$$

with the absolute value square already denoted in Eq. (16). We again assume initial condition (15) for our system. Then $c_2^+(t)$ is related to the initial state $c_0^{+,\uparrow}(t)$ by the sub-matrix element $U_{2,0}^{+s;+\uparrow}(t, 0)$ of the time-evolution operator via the general propagation equation

$$c_n^{\gamma,s}(t) = \sum_{n,n',\gamma,\gamma',s,s'} U_{n,n'}^{\gamma,s;\gamma',s'}(t, 0) c_{n'}^{\gamma',s'}(0). \tag{18}$$

The next neighbor-coupling of the interaction (13) implies the necessity of second order time-dependent perturbation theory for the lowest non-vanishing contribution

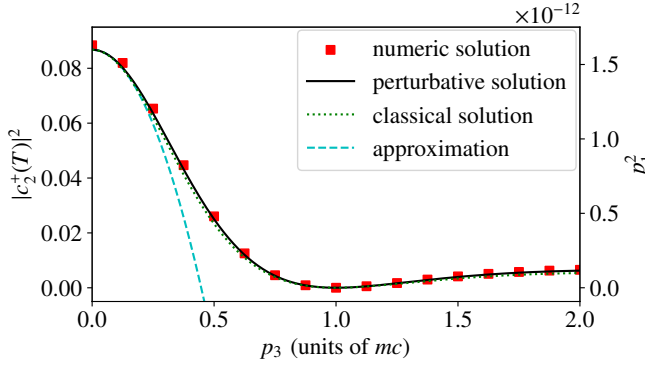


FIG. 2. Diffraction probability (16) of the two-photon Kapitza-Dirac effect as a function of the transverse electron momentum p_3 . The parameters and initial condition (15) are as for Fig. 1 with $T = 150 \times 2\pi/\omega$, where the first data point of the numeric solution at $p_3 = 0$ corresponds to the gray dot at the gray dotted time mark in Fig. 1(a). The results of the numeric solutions of the differential equation (12) are marked by red boxes and the analytic short-time solution from time-dependent perturbation theory (perturbative solution) of Eq. (30) is displayed by a solid black line. The green dotted line marks the square of the electron's classical momentum in laser propagation direction (axis on the right) for the case of the relativistic description of the classical equations of motion (87). This classical solution is performed with a vector potential amplitude of $eA = 10^{-3} mc^2$, with all other parameters being consistent with the values used for the quantum calculations. The cyan dashed line marks the low momentum approximation (51) of the perturbative relativistic quantum solution, where we mention that the relativistic classical solution (94) exhibits the same scaling with respect to the transverse momentum p_3 as the analytic quantum solution.

in $U_{2,0}^{+,s;+\uparrow}(t, 0)$. The perturbative time-evolution operator can be denoted as [24]

$$U(t, 0) = \left(-\frac{i}{\hbar} \right)^2 \int_0^t dt' \int_0^{t'} dt'' \tilde{V}(t') \tilde{V}(t''), \quad (19)$$

with the interaction V as in Eq. (13), in the interaction picture

$$\tilde{V} = e^{iH_0 t/\hbar} V e^{-iH_0 t/\hbar}. \quad (20)$$

In explicit index notion this interaction term reads as

$$\tilde{V}_{n,n'}^{\gamma,s;\gamma',s'} = V_{n,n'}^{\gamma,s;\gamma',s'} e^{i(\gamma\omega_n - \gamma'\omega_{n'})t}, \quad (21)$$

and allows us to denote Eq. (19) in the form

$$U_{2,0}^{+,s;+\uparrow}(t, 0) = \sum_{\gamma',s'} \left(-\frac{i}{\hbar} \right)^2 \int_0^t dt' \int_0^{t'} dt'' \quad (22a)$$

$$\times e^{i(\omega_2 - \gamma'\omega_1)t'} V_{2,1}^{+,s;\gamma',s'}(t') \quad (22b)$$

$$\times e^{i(\gamma'\omega_1 - \omega_0)t''} V_{1,0}^{\gamma',s';+\uparrow}(t''). \quad (22c)$$

We assume $\xi(t) = 1$ for the situation of an assumed short turn on and turn off of the standing light wave ($\Delta T \ll T$)

in Eq. (2). By substituting Eq. (13) into Eq. (22) we obtain

$$U_{2,0}^{+,s;+\uparrow}(t, 0) = \left(-\frac{i}{\hbar} \frac{eA_0}{4} \right)^2 \quad (23a)$$

$$\times \sum_{\gamma',s'} \Xi^{\gamma'} L_{2,1}^{+,s;\gamma',s'} L_{1,0}^{\gamma',s';+\uparrow}, \quad (23b)$$

with the double time-integral

$$\Xi^{\gamma} = - \int_0^t dt' \int_0^{t'} dt'' e^{i(\omega_2 - \gamma\omega_1)t'} \left(e^{i\omega t'} - e^{-i\omega t'} \right) \times e^{i(\gamma\omega_1 - \omega_0)t''} \left(e^{i\omega t''} - e^{-i\omega t''} \right). \quad (24)$$

Relevant for the population transfer of Rabi cycles in the Kapitza-Dirac effect are the non-oscillatory terms, which is a reason for us, to neglect the counter-rotating terms $e^{\pm i\omega t'} e^{\pm i\omega t''}$ and the lower limit of the t'' integral [12, 17, 23] in Eq. (24). Then for each $\gamma \in \{+,-\}$ the integrand in (24) contains the product of phases

$$e^{i(\omega_2 - \gamma\omega_1 - a\omega)t'} e^{i(\gamma\omega_1 - \omega_0 + a\omega)t''}, \quad (25)$$

with the two possibilities $a \in \{-, +\}$. The upper limit of the t'' integral evaluates to $-iF^{\gamma}$, with

$$F_a^{\gamma} = \frac{1}{\gamma\omega_1 - \omega_0 + a\omega}, \quad (26a)$$

and

$$F^{\gamma} = F_+^{\gamma} + F_-^{\gamma}. \quad (26b)$$

Note, that $\omega_2 = \omega_0$ holds and the exponential in Eq. (25) cancels, when integrating (24), due to the momentum configuration which we have imposed for obtaining classical energy and momentum conservation of the final states in the Kapitza-Dirac effect [16, 17]. The second t' integral then yields $\Xi^{\gamma} = -iF^{\gamma}t$ in Eq. (24), such that Eq. (23) can be written as

$$U_{2,0}^{+,s;+\uparrow}(t, 0) = i \left(\frac{eA_0}{4\hbar} \right)^2 t \quad (27a)$$

$$\times \sum_{\gamma',s'} F^{\gamma'} L_{2,1}^{+,s;\gamma',s'} L_{1,0}^{\gamma',s';+\uparrow}. \quad (27b)$$

This result can be associated with a semi-classical interaction picture [16, 17] as illustrated in Fig. 3, where the initial quantum state c_0^+ and final state c_2^+ correspond to

$$|e_0^-, \gamma_+\rangle = c_{p_0}^{\dagger} a_k^{\dagger} |0\rangle \quad (\text{initial}) \quad (28a)$$

$$|e_2^-, \gamma_-\rangle = c_{p_2}^{\dagger} a_{-k}^{\dagger} |0\rangle \quad (\text{final}) \quad (28b)$$

in the context of a fully quantized theory [12] of the equivalent scattering amplitudes in Compton scattering, in the context of old-fashioned perturbation theory [25, 26]. The right-hand side of Eq. (28) denotes the vacuum state

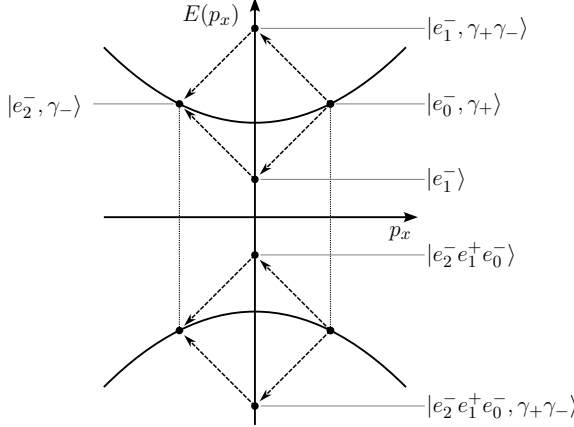


FIG. 3. Coupling paths in perturbation theory which are corresponding to the four intermediate states in Eq. (29) in the context of Compton scattering [12]. The interaction starts with the single electron e_0^- , single photon γ_+ state $|e_0^-, \gamma_+\rangle$ and also ends with a single electron e_2^- , single photon γ_- state $|e_2^-, \gamma_-\rangle$, where the electron acquires two photon momenta $0 \rightarrow 2$ and the photon momentum is reversed $+\rightarrow -$. The quantum paths in the negative energy continuum (corresponding to F_a^-) are associated with the state configuration of an electron plus an electron-positron pair $|e_2^- e_1^+ e_0^-\rangle$, $|e_2^- e_1^+ e_0^-, \gamma_+ \gamma_-\rangle$ in a fully quantized theory.

$|0\rangle$, photon creation operator a_k^\dagger and electron creation operator $c_{\mathbf{p}_n}^\dagger$ at momentum n , where we have omitted spin- and polarization degrees of freedom, for simplicity. Carrying on as in reference [12], the intermediate states in Eq. (27) with prefactors F_a^γ correspond to the quantized states

$$F_+^+ \Leftrightarrow |e_1^-\rangle = c_{\mathbf{p}_1}^\dagger |0\rangle \quad (29a)$$

$$F_+^+ \Leftrightarrow |e_1^-, \gamma_+ \gamma_-\rangle = c_{\mathbf{p}_1}^\dagger a_k^\dagger a_{-k}^\dagger |0\rangle \quad (29b)$$

$$F_+^- \Leftrightarrow |e_2^- e_1^+ e_0^-\rangle = c_{\mathbf{p}_2}^\dagger d_{\mathbf{p}_1}^\dagger c_{\mathbf{p}_0}^\dagger |0\rangle \quad (29c)$$

$$F_-^- \Leftrightarrow |e_2^- e_1^+ e_0^-, \gamma_+ \gamma_-\rangle = c_{\mathbf{p}_2}^\dagger d_{\mathbf{p}_1}^\dagger c_{\mathbf{p}_0}^\dagger a_k^\dagger a_{-k}^\dagger |0\rangle \quad (29d)$$

with positron creation operators $d_{\mathbf{p}_n}^\dagger$. In this context we mention that electronic anti-particle states are added with their positive energy to a quantized Hamiltonian in quantum field theory, by a canonical quantization procedure, for obtaining a Hamiltonian in the theory which is bound from below. Therefore, the excitation energies of the photon excitations are appearing mirrored along the energy axis in the classical single particle energy-momentum diagram in Fig. 3.

E. Coupling to negative states

Having discussed the physical interpretation of the perturbative solution (27), we now draw our attention to the aspired coupling strength of the quantum paths (29), which contribute to the diffraction probability. The diffraction probability $|c_2^+(T)|^2$ can be expanded by using

the propagation equation (18) with the matrix element from the lowest perturbative contribution (27), which results in

$$|c_2^+(T)|^2 = \sum_s \left| U_{2,0}^{+,s;+,+}(T, 0) \right|^2 \quad (30a)$$

$$= \sum_s \left| \sum_{\gamma',s'} \left(\frac{eA_0}{4\hbar} \right)^2 T F^{\gamma'} L_{2,1}^{+,s;\gamma',s'} L_{1,0}^{\gamma',s';+,+} \right|^2. \quad (30b)$$

We display this diffraction probability as black solid line in Fig. 2 as a function of the transverse momentum p_3 and find a match with the corresponding numeric solution (red boxes). The observed agreement between numeric and analytic plane-wave solutions of the relativistically described Kapitza-Dirac effect is in line with previous studies [12, 16, 17, 21].

The advantage of the perturbative solution is that it allows for isolating the contribution which involves the coupling to virtual negative states in the dynamics. To do so, we now remove the sum over the intermediate electron energy given by the index γ' and also the spin sum over the index s in the total diffraction probability in Eq. (30) and define this as the quantity

$$|c_2^{+,s}(T)|_{\gamma'}^2 = \left| \sum_{s'} \left(\frac{eA_0}{4\hbar} \right)^2 T F^{\gamma'} L_{2,1}^{+,s;\gamma',s'} L_{1,0}^{\gamma',s';+,+} \right|^2. \quad (31)$$

The object $|c_2^{+,s}(T)|_{\gamma'}^2$ with the added γ' index provides a measure about how much the positive and negative coupling path contributes to the diffraction probability, when they were not coherently interfering at detection time T of the process. The diffraction probability $|c_2^+(T)|^2$ and the coupling strengths $|c_2^{+,s}(T)|_{\gamma'}^2$ are depicted as a function of the transverse momentum p_3 in Fig. 4. We see that the coupling $|c_2^{+,+}(T)|^2$ to the intermediate negative electron states can dominate over the coupling $|c_2^{+,-}(T)|^2$ of the intermediate positive electron states by orders of magnitude, for transverse electron momenta p_3 along the laser polarization direction smaller than mc . At this point we also would like to mention that the two spin-preserving transitions (from initial spin $s' = \uparrow$ to final spin $s = \uparrow$, red dashed and blue dotted lines of the functions $|c_2^{+,\pm}(T)|_{\pm}^2$) cancel each other at $p_3 = mc$. This cancellation results in a dip in the diffraction probability $|c_2^+(T)|^2$, where only the spin-changing couplings $|c_2^{+,-}(T)|^2$ and $|c_2^{+,-}(T)|^2$ contribute to the quantum dynamics, which is the reason as to why a spin-flip in the Kapitza-Dirac effect [17] can emerge as an observable feature.

We further would like to point out once more, that the dominant coupling $|c_2^{+,-}(T)|^2$ to the negative states at small transverse momenta $p_3 < mc$ corresponds to the processes with a virtual electron-positron pair

$$|e_0^-, \gamma_+\rangle \rightarrow |e_2^- e_1^+ e_0^-\rangle \rightarrow |e_2^-, \gamma_-\rangle \quad (32a)$$

$$|e_0^-, \gamma_+\rangle \rightarrow |e_2^- e_1^+ e_0^-, \gamma_+ \gamma_-\rangle \rightarrow |e_2^-, \gamma_-\rangle, \quad (32b)$$

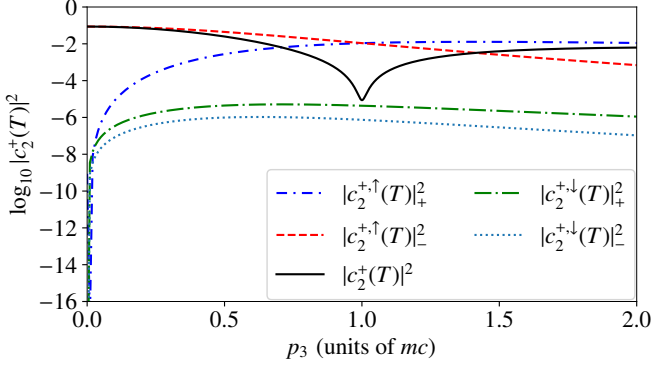


FIG. 4. Diffraction probabilities for different coupling paths of the two-photon Kapitza-Dirac effect as a function of the transverse momentum p_3 . Displayed is the perturbatively solved diffraction probability $|c_2^+(T)|^2$ from Eq. (30) and the spin resolved positive and negative coupling strengths $|c_2^{+,s}(T)|_{\gamma'}^2$ from Eq. (31). The probability $|c_2^+(T)|^2$ is the same as the black line in Fig. 2, where its shape appears differently due to the logarithmic scaling in this figure. We observe that the coupling path with a negative intermediate electron state $|c_2^{+,(T)}|_{\gamma'}^2$ is dominating the diffraction probability for $p_3 < mc$.

for the case of an ultra-low field interaction of a single photon in Compton scattering in the case of a quantized theory [12] [see particle quantum excitations introduced in Eqs. (28) and (29)]. The electron-positron pair in Eq. (32) is missing in the processes of intermediate *positive* state coupling amplitude $|c_2^{+,(T)}|_{\gamma'}^2$, which corresponds to

$$|e_0^-, \gamma_+\rangle \rightarrow |e_1^-\rangle \rightarrow |e_2^-, \gamma_-\rangle \quad (33a)$$

$$|e_0^-, \gamma_+\rangle \rightarrow |e_1^-, \gamma_+\gamma_-\rangle \rightarrow |e_2^-, \gamma_-\rangle. \quad (33b)$$

F. Low transverse momentum approximation

We now establish explicit expressions for the diffraction probability for the case of low transverse electron momenta, for comparison with the non-relativistic and classical descriptions of the quantum dynamics of the 2-photon Kapitza-Dirac effect. In order to do so, we introduce the quantities

$$g_n^+ := \frac{1}{\sqrt{2}} \left(1 + \frac{mc^2}{\mathcal{E}_n} \right)^{1/2} \quad (34a)$$

$$g_n^- := \frac{c}{\sqrt{2}} \left(\frac{1}{\mathcal{E}_n(\mathcal{E}_n + mc^2)} \right)^{1/2}, \quad (34b)$$

and based on them also

$$t_{n,n'} = g_n^+ g_{n'}^+ + \mathbf{p}_n \cdot \mathbf{p}_{n'} g_n^- g_{n'}^- \quad (35a)$$

$$s_{n,n'}^l = p_{nl} g_n^- g_{n'}^+ + p_{n'l} g_n^+ g_{n'}^- \quad (35b)$$

$$r_{n,n'}^l = p_{nl} g_n^- g_{n'}^+ - p_{n'l} g_n^+ g_{n'}^- \quad (35c)$$

$$w_{n,n'}^{lq} = p_{nl} p_{n'q} g_n^- g_{n'}^- + p_{nq} p_{n'l} g_n^- g_{n'}^-, \quad (35d)$$

where we denote the l -th component of the momentum \mathbf{p}_n as $p_{nl} = \mathbf{p}_n \cdot \mathbf{e}_l$, with the canonical unit vector \mathbf{e}_l in l -direction. On the basis of these functions, the spinor-matrix contractions (14) can be expanded as [17, 21]

$$L_{n,n'}^{+,s;+,s'} = \begin{pmatrix} s_{n,n'}^3 & -r_{n,n'}^1 \\ r_{n,n'}^1 & s_{n,n'}^3 \end{pmatrix} \quad (36a)$$

$$L_{n,n'}^{\mp,s;\pm,s'} = \begin{pmatrix} t_{n,n'} - w_{n,n'}^{33} & -w_{n,n'}^{31} \\ -w_{n,n'}^{31} & -t_{n,n'} + w_{n,n'}^{33} \end{pmatrix}, \quad (36b)$$

where the columns and rows of the matrices on the right-hand side are indexed by the spinor indices s' and s , respectively. With these matrices, the expression in Eq. (27b) can be reformulated as

$$F^+ s_{2,1}^3 s_{1,0}^3 - F^+ r_{2,1}^1 r_{1,0}^1 \quad (37a)$$

$$+ F^-(t_{2,1} - w_{2,1}^{33})(t_{1,0} - w_{1,0}^{33}) + F^- w_{2,1}^{31} w_{1,0}^{31} \quad (37b)$$

for the final spin index $s = \uparrow$ and

$$F^+ s_{2,1}^3 r_{1,0}^1 + F^+ r_{2,1}^1 s_{1,0}^3 \quad (38a)$$

$$+ F^-(t_{2,1} - w_{2,1}^{33})w_{1,0}^{31} - F^- w_{2,1}^{31}(t_{1,0} - w_{1,0}^{33}) \quad (38b)$$

for the final spin index $s = \downarrow$. The upper lines Eqs. (37a) and (38a) are contributions with the intermediate state energy index $\gamma' = +$ and the lower lines Eqs. (37b) and (38b) are contributions with $\gamma' = -$. Our aim is now to deduce simplified expressions for Eqs. (37) and (38), for small momenta p_3 , with the following hierarchy of magnitudes

$$\frac{\hbar k_L}{mc} \ll \frac{p_3}{mc} \ll 1, \quad (39)$$

or in a simpler notion $\hbar k_L \ll p_3 \ll mc$. The laser photon energy $\hbar k_L$ over the electron rest-mass energy mc^2 is on the percent level for hard x-ray lasers and on the order of 10^{-6} for optical lasers, such that the assumed order (39) appears justified. Having in mind that $\hbar k_L \ll p_3$, we start with the second order Taylor expansion of g_n^+ with respect to p_3

$$g_n^+ \approx 1 - \frac{1}{8} \frac{p_3^2}{m^2 c^2}, \quad (40)$$

where we later also need the product of these coefficients, which are approximately

$$g_n^+ g_{n'}^+ \approx 1 - \frac{1}{4} \frac{p_3^2}{m^2 c^2}. \quad (41)$$

Regarding the coefficients g_n^- we only keep the zeroth order of the series expansion

$$g_n^- \approx \frac{1}{2mc}, \quad (42)$$

which we justify by the observation that the g_n^- only appear together with components of the electron momenta

$\mathbf{p}_n = [(n-1)\hbar k_L, 0, p_3]^T$, specifically

$$p_{n1} g_n^- \approx \frac{(n-1)\hbar k_L}{2mc} \quad (43a)$$

$$p_{n3} g_n^- \approx \frac{p_3}{2mc}. \quad (43b)$$

Since we have $\hbar k_L \ll p_3$, Eq. (43a) can be neglected, if compared with Eq. (43b). For the same reason we can approximate the product of momenta \mathbf{p}_n and $\mathbf{p}_{n'}$ as

$$\mathbf{p}_n \cdot \mathbf{p}_{n'} = (n-1)(n'-1)\hbar^2 k_L^2 + p_3^2 \approx p_3^2, \quad (44)$$

and consequently

$$\mathbf{p}_n \cdot \mathbf{p}_{n'} g_n^- g_{n'}^- \approx \frac{1}{4} \frac{p_3^2}{m^2 c^2}. \quad (45)$$

We can now approximate (35a) up to order p_3^2 as

$$t_{n,n'} \approx 1, \quad (46a)$$

where Eqs. (41) and (45) were substituted. Similarly, the other relevant expressions in Eqs. (35) can be written as

$$s_{n,n'}^3 \approx \frac{p_3}{mc} \quad (46b)$$

$$r_{n,n'}^1 \approx \frac{(n-n')\hbar k_L}{2mc} \quad (46c)$$

$$w_{n,n'}^{31} \approx \frac{(n+n'-2)\hbar k_L p_3}{4m^2 c^2} \quad (46d)$$

$$w_{n,n'}^{33} \approx \frac{p_3^2}{2m^2 c^2}. \quad (46e)$$

It remains to find approximations for the coefficients F^γ , because the F^γ also appear in the expressions (37) and (38), which we want to approximate. We first note, that we can simplify the sum (26b) into

$$F^\gamma = \frac{2\hbar(\gamma\mathcal{E}_1 - \mathcal{E}_0)}{(\gamma\mathcal{E}_1 - \mathcal{E}_0)^2 - \hbar^2\omega^2} = \frac{2\hbar(\gamma\mathcal{E}_1 - \mathcal{E}_0)}{2\mathcal{E}_1(\mathcal{E}_1 - \gamma\mathcal{E}_0)} = \gamma \frac{\hbar}{\mathcal{E}_1}, \quad (47)$$

where we manipulated a term in the denominator into

$$(\gamma\mathcal{E}_1 - \mathcal{E}_0)^2 = \mathcal{E}_1^2 + \mathcal{E}_0^2 - 2\gamma\mathcal{E}_0\mathcal{E}_1 = 2\mathcal{E}_1^2 + \hbar^2\omega^2 - 2\gamma\mathcal{E}_0\mathcal{E}_1 \quad (48)$$

and inserted a factor $\gamma^2 = 1$ in the denominator before the last equality in (47). Finally, the Taylor expansion of Eq. (47) yields

$$F^\gamma = \gamma \frac{\hbar}{mc^2} \left(1 - \frac{1}{2} \frac{p_3^2}{m^2 c^2} \right). \quad (49)$$

With these approximations, we observe that the spin-preserving expression (37) dominates by a factor $p_3/(\hbar k_L)$ over the spin flipping expression (38), such that we assume (38) to be negligible. Therefore, we can write the dominant contribution in Eq. (27) as

$$U_{2,0}^{+, \uparrow; +, \uparrow}(t, 0) = -i \frac{e^2 A_0^2 t}{16mc^2 \hbar} \left(1 - \frac{5}{2} \frac{p_3^2}{m^2 c^2} \right), \quad (50)$$

by inserting the largest terms in Eqs. (46a), (46e) and (49) into Eq. (37). Eq. (50) allows us to write the short time diffraction probability (30a) up to quadratic order in $p_3/(mc)$ as

$$|c_2^+(T)|^2 \approx \left(\frac{e^2 A_0^2 t}{16mc^2 \hbar} \right)^2 \left(1 - 5 \frac{p_3^2}{m^2 c^2} \right), \quad (51)$$

which we include as cyan dashed line in Fig. 2. From the figure we conclude a good agreement between the perturbative solution (30) and its approximation for small transverse momenta (51). We can further confirm the approximation of the short time solution of predicted Rabi oscillations [22, 24] in Kapitza-Dirac scattering [14–17]

$$|c_0^+(t)|^2 = \cos^2 \left(\frac{\Omega_R t}{2} \right) \quad (52a)$$

$$|c_2^+(t)|^2 = \sin^2 \left(\frac{\Omega_R t}{2} \right), \quad (52b)$$

where the Rabi frequency at $p_3 = 0$ can be identified from Eq. (50) as

$$\Omega_R = \frac{e^2 A_0^2}{8mc^2 \hbar}. \quad (53)$$

For the parameter $eA_0 = 0.01 mc^2$ in Fig. 1 this results in $\Omega_R = 1.25 \times 10^{-5} mc^2/\hbar$. The corresponding Rabi period

$$T_R = \frac{2\pi}{\Omega_R} = 5.03 \times 10^5 \frac{\hbar}{mc^2} = 1600 \frac{2\pi}{\omega} \quad (54)$$

matches the oscillation period in Fig. 1(a) and is another confirmation for our approximation of the perturbative calculation.

After having verified the validity of the perturbative solution and its approximation, we want to emphasize again that it is the contribution (37b) with scaling

$$F^-(t_{2,1} - w_{2,1}^{33})(t_{1,0} - w_{1,0}^{33}) \approx 1 - \frac{3}{2} \frac{p_3^2}{m^2 c^2}, \quad (55)$$

which dominates the quantum dynamics for small and in particular zero transverse electron momenta $p_3 = 0$ in the two-photon Kapitza-Dirac effect. This is of significant relevance, because the term (37b) arises from coupling to *negative* states [ie. $\gamma' = -$ in Eq. (27b)] and is therefore to be associated with the coupling process (32), in which a virtual electron-positron pair is involved in the context of Compton scattering in a fully quantized theory.

III. NON-RELATIVISTIC QUANTUM DESCRIPTION

A. Schrödinger equation

In the following, we want to compare corresponding expressions of the diffraction probability from non-relativistic and also classical theory, in the hope to acquire more intuition for the dynamics of the process of interest. We start considering the non-relativistic quantum

description in terms of the Schrödinger equation. When coupled to the vector potential only, the single component Hamiltonian of the Schrödinger equation reads

$$H = \frac{1}{2m} \left(\mathbf{p} - \frac{e}{c} \mathbf{A} \right)^2, \quad (56)$$

with the time-evolution implied by Eq. (3). As in the relativistic case, we split the Hamiltonian (56) again into a kinetic term H_0 and an interaction term V by

$$H_0 = \frac{\mathbf{p}^2}{2m} \quad (57a)$$

$$V = \frac{e^2 \mathbf{A}^2}{2mc^2} - \frac{e \mathbf{A} \cdot \mathbf{p}}{mc}, \quad (57b)$$

where the contribution $\mathbf{p} \cdot \mathbf{A}$ with \mathbf{p} acting at \mathbf{A} is zero for the assumed vector potential (1).

In the non-relativistic case, the frequencies $\omega_n = \mathcal{E}_n/\hbar$ with momenta $\mathbf{p}_n = [(n-1)\hbar k_k, 0, p_3]^T$ are now given by the energy eigenvalues of (57a) as

$$\mathcal{E}_n = \frac{(n-1)^2 \hbar^2 k_L^2}{2m} + \frac{p_3^2}{2m}. \quad (58)$$

Analogously, we expand the wave function $\Psi(\mathbf{x}, t)$ as

$$\Psi(\mathbf{x}, t) = \sum_n c_n(t) \psi_n(\mathbf{x}), \quad (59)$$

with the single component plane waves

$$\psi_n(\mathbf{x}) = \sqrt{\frac{k_L}{2\pi}} e^{i\mathbf{p}_n \cdot \mathbf{x}}. \quad (60)$$

B. Perturbative solution

A system of differential equations for the Schrödinger Hamiltonian (56) for the expansion coefficients $c_n(t)$ similarly to (12) can be established [21], with the interaction operator matrix elements in discrete momentum space

$$V_{n,n'} = \frac{1}{\lambda} \int_{-\lambda/2}^{\lambda/2} d\mathbf{x} \psi_n^*(\mathbf{x}) \left[\frac{e^2 \mathbf{A}^2}{2mc^2} - \frac{e \mathbf{A} \cdot \mathbf{p}}{mc} \right] \psi_{n'}(\mathbf{x}) = \frac{e^2 A_0^2 \sin^2(\omega t) \xi^2(t)}{8mc^2} (\delta_{n,n'-2} + 2\delta_{n,n'} + \delta_{n,n'+2}) \quad (61a)$$

$$- \frac{e A_0 p_3 \sin(\omega t) \xi(t)}{2mc} (\delta_{n,n'-1} + \delta_{n,n'+1}). \quad (61b)$$

We are interested in using the interaction (61) for obtaining the perturbative solution of $U_{2,0}$ for the case of the Schrödinger equation. Second next neighbor coupling arises in Eq. (61a), where the vector potential enters the Hamiltonian quadratically. This implies non-vanishing contributions also from first order time-dependent perturbation theory [24]

$$U^{\text{st}}(t, 0) = \left(-\frac{i}{\hbar} \right) \int_0^t dt' \tilde{V}(t'), \quad (62)$$

which can be written as

$$U_{2,0}^{\text{st}}(t, 0) = \left(-\frac{i}{\hbar} \right) \int_0^t dt' e^{i(\omega_2 - \omega_0)t'} V_{2,0}(t') \quad (63)$$

in the component notion of the interaction picture. As for the relativistic case, we have $\omega_2 = \omega_0$ and with setting $\xi(t) = 1$, the only relevant matrix element in the interaction (61) results in

$$U_{2,0}^{\text{st}}(t, 0) = \left(-\frac{i}{\hbar} \right) \left(\frac{e^2 A_0^2}{8mc^2} \right) \int_0^t dt' \sin^2(\omega t'). \quad (64)$$

The \sin^2 integral evaluates to $t/2$ for integration times equal to multiples of a half laser period $t = n\pi/\omega$, $n \in \mathbb{N}$. Since the oscillatory part of the integral gets negligibly small as compared to the integral value for large times t , we can approximate

$$U_{2,0}^{\text{st}}(t, 0) \approx -i \frac{e^2 A_0^2 t}{16mc^2 \hbar}. \quad (65)$$

The next-neighbor coupling in (61b) also implies a lowest order non-vanishing contribution for $U_{2,0}$ in second order time-dependent perturbation theory

$$U_{2,0}^{\text{nd}}(t, t_0) = \left(-\frac{i}{\hbar} \right)^2 \int_{t_0}^t dt' \int_{t_0}^{t'} dt'' \times e^{i(\omega_2 - \omega_1)t'} V_{2,1}(t') e^{i(\omega_1 - \omega_0)t''} V_{1,0}(t''). \quad (66)$$

Setting again $\xi(t) = 1$ results in

$$U_{2,0}^{\text{nd}}(t, 0) = - \left(\frac{e A_0 p_3}{4mc\hbar} \right)^2 \Xi^+, \quad (67)$$

where we reuse expression (24) for the time integral. However, with the non-relativistic energies (58), the denominator in (26a) turns into

$$\omega_1 - \omega_0 + a\omega = -\frac{\hbar k_L^2}{2m} + a c k_L = -\frac{k_L}{2m} (\hbar k_L - 2amc) \quad (68)$$

such that the sum (26b) can be approximated as

$$F^+ = -\frac{2m}{k_L} \left(\frac{1}{\hbar k_L - 2mc} + \frac{1}{\hbar k_L + 2mc} \right) = -\frac{2m}{k_L} \frac{2\hbar k_L}{\hbar^2 k_L^2 - 4m^2 c^2} \approx \frac{\hbar}{mc^2}, \quad (69)$$

where we assume $\hbar k_L \ll mc$. Inserting $-iF^+$ as solution of Ξ^+ into Eq. (67) results in

$$U_{2,0}^{\text{nd}}(t, 0) = i \frac{e^2 A_0^2 p_3^2}{16m^3 c^4 \hbar}. \quad (70)$$

Finally, the sum of first and second order perturbation in non-relativistic quantum theory can be written as

$$U_{2,0}(t, 0) = U_{2,0}^{\text{st}}(t, 0) + U_{2,0}^{\text{nd}}(t, 0) \approx -i \frac{e^2 A_0^2 t}{16mc^2 \hbar} \left(1 - \frac{p_3^2}{m^2 c^2} \right). \quad (71)$$

This appears to be an expression, which is of similar form as the relativistic solution (50), however with a different functional dependence of the transverse momentum p_3 .

IV. NON-RELATIVISTIC CLASSICAL DESCRIPTION

The classical motion of an electron in a standing light wave leads to an effective ponderomotive potential, which can be directly related to the electron diffraction process in the Kapitza-Dirac effect [14, 15, 27], where we follow and extend the calculation in references [14, 15] in the following. We begin the derivation of the ponderomotive potential with the Lorentz force

$$\mathbf{F} = e \left[\mathbf{E}(\mathbf{x}, t) + \frac{\mathbf{p}}{mc} \times \mathbf{B}(\mathbf{x}, t) \right], \quad (72)$$

which the electron as classical, point-like particle is subject to. The electric and magnetic fields in the Lorentz force are implied by the vector potential (1), through the relations [28]

$$\mathbf{E}(\mathbf{x}, t) = -\frac{1}{c} \frac{\partial \mathbf{A}}{\partial t} = -A_0 k_L \cos(k_L x) \cos(\omega t) \mathbf{e}_3 \quad (73a)$$

$$\mathbf{B}(\mathbf{x}, t) = \nabla \times \mathbf{A} = A_0 k_L \sin(k_L x) \sin(\omega t) \mathbf{e}_2, \quad (73b)$$

for the situation with $\xi(t) = 1$. For an initial particle momentum $\mathbf{p} = p_3 \mathbf{e}_3$ and the corresponding initial position trajectory $\mathbf{x} = (x, y, z + p_3 t/m)$ this yields

$$\begin{aligned} \mathbf{F} = -e A_0 k_L \cos(k_L x) \cos(\omega t) \mathbf{e}_3 \\ - \frac{e A_0 k_L p_3}{mc} \sin(k_L x) \sin(\omega t) \mathbf{e}_1. \end{aligned} \quad (74)$$

The Lorentz force (72) implies the modified particle momentum

$$\begin{aligned} \tilde{\mathbf{p}} = \int \mathbf{F}(t') dt' = & \left[-\frac{e A_0}{c} \cos(k_L x) \sin(\omega t) + p_3 \right] \mathbf{e}_3 \\ & + \frac{e A_0 p_3}{mc^2} \sin(k_L x) \cos(\omega t) \mathbf{e}_1 \end{aligned} \quad (75)$$

and consequently also the modified particle position

$$\begin{aligned} \tilde{\mathbf{x}} = \int \frac{\tilde{\mathbf{p}}(t')}{m} dt' = & \mathbf{x} + \frac{e A_0}{k_L m c^2} \cos(k_L x) \cos(\omega t) \mathbf{e}_3 \\ & + \frac{e A_0 p_3}{k_L m^2 c^3} \sin(k_L x) \sin(\omega t) \mathbf{e}_1. \end{aligned} \quad (76)$$

Here, we assume that except the original particle position \mathbf{x} and momentum \mathbf{p} no further additional integration constants arise when computing the anti-derivatives, for the case that the electron was adiabatically entering the laser field in the distant past. The oscillations

$$\delta \mathbf{x} = \tilde{\mathbf{x}} - \mathbf{x}, \quad \delta \mathbf{p} = \tilde{\mathbf{p}} - \mathbf{p}, \quad (77)$$

are now emerging in Eqs. (75) and (76), if compared to the original position \mathbf{x} and momentum \mathbf{p} . At these updated positions, the electro-magnetic fields can be approximated as

$$\tilde{\mathbf{E}} = \mathbf{E}(\tilde{\mathbf{x}}, t) \approx \mathbf{E}(\mathbf{x}, t) + \delta \mathbf{E} \quad (78a)$$

$$\tilde{\mathbf{B}} = \mathbf{B}(\tilde{\mathbf{x}}, t) \approx \mathbf{B}(\mathbf{x}, t) + \delta \mathbf{B}. \quad (78b)$$

The small quantities $\delta \mathbf{E}$ and $\delta \mathbf{B}$ are taken as the terms of a first order Taylor expansion of the electro-magnetic field, which contains the field derivatives

$$\frac{\partial}{\partial x} \mathbf{E}(\mathbf{x}, t) = A_0 k_L^2 \sin(k_L x) \cos(\omega t) \mathbf{e}_3 \quad (79a)$$

$$\frac{\partial}{\partial x} \mathbf{B}(\mathbf{x}, t) = A_0 k_L^2 \cos(k_L x) \sin(\omega t) \mathbf{e}_2. \quad (79b)$$

We can thus combine

$$\delta \mathbf{E} = \delta x \frac{\partial}{\partial x} \mathbf{E} = \frac{e A_0^2 k_L p_3}{m^2 c^3} \sin^2(k_L x) \sin(\omega t) \cos(\omega t) \mathbf{e}_3, \quad (80a)$$

$$\delta \mathbf{B} = \delta x \frac{\partial}{\partial x} \mathbf{B} = \frac{e A_0^2 k_L p_3}{m^2 c^3} \sin(k_L x) \cos(k_L x) \sin^2(\omega t) \mathbf{e}_2. \quad (80b)$$

Therefore, the fields $\tilde{\mathbf{E}}$ and $\tilde{\mathbf{B}}$ at the updated position $\tilde{\mathbf{x}}$ and momentum $\tilde{\mathbf{p}}$ result in the modified force

$$\tilde{\mathbf{F}} \approx e \left[\mathbf{E} + \delta \mathbf{E} + \frac{\mathbf{p} + \delta \mathbf{p}}{mc} \times (\mathbf{B} + \delta \mathbf{B}) \right]. \quad (81)$$

The ponderomotive force, which we want to discuss here, is associated with the average of the force (81) over one laser cycle

$$\langle \tilde{\mathbf{F}} \rangle = \frac{\omega}{2\pi} \int_{t_0}^{t_0 + \frac{2\pi}{\omega}} \tilde{\mathbf{F}} dt. \quad (82)$$

We see that the cycle averages for the terms $\langle \mathbf{E} \rangle$, $\langle \delta \mathbf{E} \rangle$ and $\langle \mathbf{p} \times \mathbf{B} \rangle$ in the expansion of (81) are zero. The contribution $\langle \delta \mathbf{p} \times \delta \mathbf{B} \rangle$ is the only term which scales with the third power of the small quantity A_0 , and we neglect it for this reason. It remains

$$\langle \tilde{\mathbf{F}} \rangle \approx \frac{\omega}{2\pi} \int_{t_0}^{t_0 + \frac{2\pi}{\omega}} \frac{e}{mc} (\delta \mathbf{p} \times \mathbf{B} + \mathbf{p} \times \delta \mathbf{B}) dt \quad (83a)$$

$$= \frac{k_L e^2 A_0^2}{mc^2} \left(1 - \frac{p_3^2}{m^2 c^2} \right) \sin(k_L x) \cos(k_L x) \mathbf{e}_1 \quad (83b)$$

$$\times \frac{\omega}{2\pi} \int_{t_0}^{t_0 + \frac{2\pi}{\omega}} \sin^2(\omega t) dt \quad (83c)$$

$$= \frac{k_L e^2 A_0^2}{2mc^2} \left(1 - \frac{p_3^2}{m^2 c^2} \right) \sin(k_L x) \cos(k_L x) \mathbf{e}_1, \quad (83d)$$

where the cycle average of the transverse component of $\langle \delta \mathbf{p} \times \mathbf{B} \rangle$ is zero as well.

The ponderomotive force expression (83d) has some similarities with the non-relativistic perturbative solution (71) of the Schrödinger equation. Consequently, and consistent with the considerations in reference [27], we show in the following that (83d) actually causes the same quantum state propagation expression (71), by computing the ponderomotive potential from the ponderomotive force, and then calculating the time-evolution which is implied by the potential. The ponderomotive potential is obtained by integrating the ponderomotive force along the

direction of the only non-trivial spacial dependence (ie. along the laser propagation direction), which yields

$$V_{\text{pond}} = - \int \langle \tilde{\mathbf{F}} \rangle \cdot \mathbf{e}_1 dx \\ = \frac{e^2 A_0^2}{4mc^2} \left(1 - \frac{p_3^2}{m^2 c^2} \right) \cos^2(k_L x). \quad (84)$$

Computing the momentum space matrix elements of this ponderomotive potential similarly to the procedure in Eq. (61a) results in the expressions

$$V_{n,n'}^{\text{pond}} = \frac{1}{\lambda} \int_{-\lambda/2}^{\lambda/2} d\mathbf{x} \psi_n^*(\mathbf{x}) V_{\text{pond}} \psi_{n'}(\mathbf{x}) \quad (85) \\ = \frac{e^2 A_0^2}{16mc^2} \left(1 - \frac{p_3^2}{m^2 c^2} \right) (\delta_{n,n'-2} + 2\delta_{n,n'} + \delta_{n,n'+2}).$$

The first order time-dependent perturbation theory expression of Eq. (85) then yields

$$U_{2,0}^{\text{st}}(t, 0) = \left(-\frac{i}{\hbar} \right) \int_0^t dt' e^{i(\omega_2 - \omega_0)t'} V_{2,0}^{\text{pond}} \\ = -i \frac{e^2 A_0^2 t}{16mc^2 \hbar} \left(1 - \frac{p_3^2}{m^2 c^2} \right), \quad (86)$$

which is indeed consistent with the result (71) of the non-relativistic perturbative quantum calculation in section III B.

V. RELATIVISTIC CLASSICAL DESCRIPTION

The non-relativistic results (71) and (86) for the electron dynamics are not consistent with the relativistic quantum solution in (50), which is a reason to investigate the relativistic classical motion of the electron as well. A literature discussion about the relativistic ponderomotive potential exists [29–33]. In this article, we follow the layout from Batelaan for the ponderomotive calculation [14, 15] which is specifically designed for Kapitza-Dirac dynamics and which we extend from the previous section IV. Our aim is, to discuss where corrections of the relativistic equations of motion occur in the non-relativistic limit of the calculation. The classical motion of an electron in a relativistic framework [28] can be denoted in the lab-frame by the coupled differential equations

$$\frac{d\mathbf{p}}{dt} = \mathbf{F} = e \left[\mathbf{E}(\mathbf{x}, t) + \frac{\mathbf{p}}{\gamma(\mathbf{p})mc} \times \mathbf{B}(\mathbf{x}, t) \right], \quad (87a)$$

$$\frac{d\mathbf{x}}{dt} = \frac{\mathbf{p}}{\gamma(\mathbf{p})m}. \quad (87b)$$

Eq. (87a) originates from a covariant formulation of the Lorentz force and generalizes the Lorentz force (72). The right-hand side of Eq. (87b) originates from the four-velocity and four-momentum, with $\mathbf{p} = m\gamma\mathbf{v}$ with respect

to lab-time t . The relativistic gamma factor

$$\gamma(\mathbf{p}) = \sqrt{1 + \frac{\mathbf{p}^2}{mc^2}} \quad (88)$$

is implied from (11) and $E = \gamma mc^2$. We numerically solve the dynamics of the classical relativistic electron trajectory according to Eqs. (87) for parameters at which the non-linear contributions to the electron dynamics appear to be small. Suitable parameters for the potential (1) with envelope (2) are $qA_0 = 10^{-3} mc^2$, $\hbar k_L = 0.02 mc$, $T = 150 \times 2\pi/\omega$ and $\Delta T = 10 \times 2\pi/\omega$. The initial particle position is $x = \lambda/8$, at a location of the periodic laser field, where we know from the non-relativistic calculation that the ponderomotive deflection is largest. We further set the initial particle parameters $y = z = 0$ and $\mathbf{p} = p_3 \mathbf{e}_3$ for the numeric simulation. The result of the numeric calculation is displayed in Fig. 2 as green dotted line, where we know from the calculation in Eqs. (83)-(86) that the ponderomotive amplitude (which is proportional to p_1) converts into a diffraction amplitude. The diffraction amplitude, in turn, converts further into a diffraction probability by taking the absolute value square of the wave function or equivalently its propagation equation (18), which is then proportional to p_1^2 . Therefore, we display p_1^2 at the ending time T of the numerical particle trajectory simulation in Fig. 2, and find proper agreement with the relativistic quantum solutions.

Having evidence, that the classical equations of motion (87) appear to be consistent with the quantum solutions, we would like to point out where the non-relativistic limit of the dynamics leads to relativistic corrections in the non-relativistic dynamics as described in the previous section. Details of this calculation appear in the more verbose calculation description in the supplemental material [34]. The difference of the relativistic equations of motion (87) as compared to the classical ones in Eqs. (72), (75) and (76) is the inverse gamma factor

$$\gamma^{-1}(\tilde{\mathbf{p}}) \approx 1 - \frac{\tilde{p}_1^2}{2m^2 c^2} - \frac{\tilde{p}_3^2}{2m^2 c^2} + \frac{3\tilde{p}_1^2 \tilde{p}_3^2}{4m^4 c^4}. \quad (89)$$

For the motion in first order (75) the gamma factor evaluates as

$$\gamma^{-1}(\tilde{\mathbf{p}}) \approx 1 - \frac{e^2 A_0^2 p_3^2}{2m^4 c^6} \sin^2(k_L x) \cos^2(\omega t) - \frac{p_3^2}{2m^2 c^2} \\ - \frac{e^2 A_0^2}{2m^2 c^4} \cos^2(k_L x) \sin^2(\omega t) + \frac{e A_0 p_3}{m^2 c^3} \cos(k_L x) \sin(\omega t), \quad (90)$$

where we neglect terms of order $\mathcal{O}(p_3^3)$ and $\mathcal{O}(A_0^3)$ and higher. In what follows, the updated x -component of the particle position $\tilde{\mathbf{x}}$ is of relevance, as this determines the x -dependent variation of the electro-magnetic field, in the derivation of the ponderomotive force. Thus, by integrating the particle position according to Eq. (87b),

we obtain the expression

$$\delta x = \frac{eA_0p_3}{k_L m^2 c^3} \sin(k_L x) \sin(\omega t) \quad (91a)$$

$$+ \frac{e^2 A_0^2 p_3^2}{2k_L m^4 c^6} \cos(k_L x) \sin(k_L x) \sin^2(\omega t), \quad (91b)$$

which is to be matched and compared with the x -component of the non-relativistic expression (76). The new term in (91b) still needs to be multiplied with the electro-magnetic fields in subsequent calculation steps and will result in terms $\mathcal{O}(A_0^3)$, which we neglect. Therefore, (91b) from the expansion (89) of the relativistic gamma factor $\gamma^{-1}(\tilde{\mathbf{p}})$ does not give any extra contributions for the ponderomotive force.

The inverse gamma factor introduces a second relativistic correction, which appears in the $\tilde{\mathbf{p}}\gamma(\tilde{\mathbf{p}})^{-1}$ expression of the Lorentz force (87a)

$$\frac{\tilde{\mathbf{p}}}{\gamma(\tilde{\mathbf{p}})} = \mathcal{A} + \mathcal{B} + \mathcal{C} + \mathcal{D} + \mathcal{F} + \mathcal{G} + \mathcal{O}(p_3^3) + \mathcal{O}(A_0^3), \quad (92)$$

with terms

$$\mathcal{A} = \frac{eA_0p_3}{mc^2} \sin(k_L x) \cos(\omega t) \mathbf{e}_1, \quad (93a)$$

$$\mathcal{B} = \frac{e^2 A_0^2 p_3^2}{m^3 c^5} \sin(k_L x) \cos(k_L x) \sin(\omega t) \cos(\omega t) \mathbf{e}_1, \quad (93b)$$

$$\mathcal{C} = p_3 \mathbf{e}_3, \quad (93c)$$

$$\mathcal{D} = -\frac{3e^2 A_0^2 p_3}{2m^2 c^4} \cos^2(k_L x) \sin^2(\omega t) \mathbf{e}_3, \quad (93d)$$

$$\mathcal{F} = \frac{3eA_0p_3^2}{2m^2 c^3} \cos(k_L x) \sin(\omega t) \mathbf{e}_3, \quad (93e)$$

$$\mathcal{G} = -\frac{eA_0}{c} \cos(k_L x) \sin(\omega t) \mathbf{e}_3. \quad (93f)$$

The relevant contributions for the time-averaged ponderomotive force of Eq. (87a) consist of the three expressions

$$\begin{aligned} \langle \tilde{\mathbf{F}} \rangle &= \frac{e}{mc} (\langle \mathcal{F} \times \mathbf{B} \rangle + \langle \mathcal{G} \times \mathbf{B} \rangle + \langle \mathcal{C} \times \delta\mathbf{B} \rangle) \\ &= \left[\frac{e^2 A_0^2 k_L}{2mc^2} \left(1 - \frac{5}{2} \frac{p_3^2}{m^2 c^2} \right) \sin(k_L x) \cos(k_L x) \right] \mathbf{e}_1, \end{aligned} \quad (94)$$

after eliminating vanishing terms and omitting higher-order powers of p_3 and A_0 as discussed in the comprehensive derivation of the ponderomotive potential in the supplemental material [34]. Following the steps (84)-(86) yields the same type of matrix element for the time-evolution operator $U_{2,0}(t, 0)$ as in the relativistic quantum calculation (50), but now with the correct factor $5/2$ in front of the reduced momentum $[p_3/(mc)]^2$. A comparison with (83) reveals that $\langle \mathcal{F} \times \mathbf{B} \rangle$ is the new contribution from the relativistic classical calculation, which provides the matching relativistic correction to the non-relativistic result and stems from the gamma factor (90).

VI. DISCUSSION

We have performed quantum and classical calculations with relativistic and non-relativistic equations of motion for the two-photon Kapitza-Dirac effect. Only the relativistic quantum calculation in section II with the Dirac equation allows for the investigation of negative intermediate states in comparison to positive intermediate states. Interesting is their different interpretation circumstance: The situation of positive intermediate states in the contribution (37a) could be matched to a classical interpretation of motion. In contrast, the contribution (37b) is putting an additional obstacle on the attempt of an intuitive understanding of the process, since (37b) originates from the coupling to negative electron states, which does not exist in classical theory. We further observe that the transverse velocity dependence of the diffraction amplitude (50) in relativistic quantum theory is contributed by the $s_{n,n'}^3$ term (37a) of positive intermediate state coupling, which can be associated with the $\mathbf{A} \cdot \mathbf{p}$ contribution to the dynamics from the Schrödinger equation in non-relativistic quantum theory. This $\mathbf{A} \cdot \mathbf{p}$ contribution, however, matches the $\mathbf{p} \times \delta\mathbf{B}$ contribution of the classical motion in the non-relativistic description and the $\langle \mathcal{C} \times \mathbf{B} \rangle$ contribution in the relativistic description. One may thus identify the positive intermediate state coupling in the relativistic quantum theory with the classical motion of a deflected electron trajectory component along the laser propagation direction, which causes the variation of the magnetic field $\delta\mathbf{B}$.

Still, it is *only* the negative state coupling (37b), which contributes an expression in the diffraction amplitude (50), which is partially independent of the transverse velocity p_3 ! This negative state coupling contribution can be associated with the \mathbf{A}^2 term in the Schrödinger equation, which in turn matches the resulting diffraction probability component of the $\delta\mathbf{p} \times \mathbf{B}$ motion of the ponderomotive potential in the non-relativistic case and $\langle (\mathcal{F} + \mathcal{G}) \times \mathbf{B} \rangle$ in the relativistic case. We emphasize that the term $\delta\mathbf{p} \times \mathbf{B}$ (or $\langle (\mathcal{F} + \mathcal{G}) \times \mathbf{B} \rangle$, respectively) corresponds to the ‘conventional’ classical motion component of the electron along the electric field, which causes the ponderomotive potential from the Lorentz force, as described by Batelaan [14, 15].

In order to summarize the similarities of the terms in non-relativistic and relativistic quantum- and classical theory, we need to distinguish between the situation of small transverse momenta ($p_3 \ll mc$) along the laser polarization direction and the situation of relativistic transverse momenta ($p_3 \gg mc$) in the Kapitza-Dirac effect. For a descriptive interpretation we want to consider a frame of reference, where the electron is reversing its momentum \mathbf{p} in the context of an analogous Compton scattering process. In such an electron centered frame, the photon performs a head-on collision for the $p_3 = 0$ situation, as sketched in Fig. 5(a). However, the photon scatters off the electron at a larger angle ϑ for the situation with $p_3 \gg mc$, as illustrated in Fig. 5 (b).

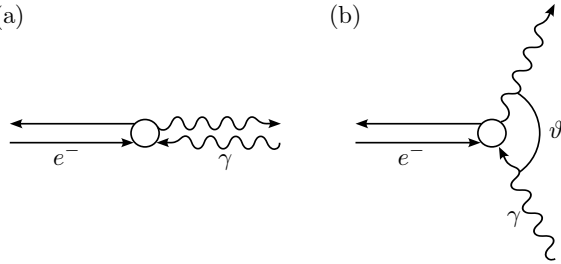


FIG. 5. Interaction geometry of Compton scattering, in a frame of reference in which the electron is reversing its momentum \mathbf{p} . (a) In this reference frame the photon is back-scattering by 180° for a situation of the Kapitza-Dirac effect with zero transverse momentum $p_3 = 0$. (b) In contrast, the photon scatters off by some angle ϑ for situations with large transverse momenta $p_3 \gg mc$ in the Kapitza-Dirac effect.

A. Small transverse electron momentum $p_3 \ll mc$ situation in Fig. 5(a)

We can make a series of statements about properties of the investigated negative state coupling for the two distinct scenarios in Fig. 5, for which in Fig. 5(a), ie. $p_3 \ll mc$ the following properties can be associated with each other:

1. The coupling to negative intermediate states [red dashed line in Fig. 4 and (37b) in the low transverse momentum approximation] in the electron-light interaction of the Kapitza-Dirac effect dominates over the coupling to positive intermediate states [blue dash-dotted line and (37a)].
2. A virtual electron-position pair [corresponding to $|e_2^- e_1^+ e_0^- \rangle$ and $|e_2^- e_1^+ e_0^-, \gamma_+ \gamma_- \rangle$ in Eq. (32)] dominantly contributes to the scattering dynamics in Compton scattering in the context of a fully quantized theory.
3. The first order time-dependent perturbative expression \mathbf{A}^2 [U^{st} in Eqs. (62)-(65)] in the expansion of $(\mathbf{p} - e\mathbf{A}/c)^2$ of the Schrödinger equation is dominating the diffraction dynamics of the Kapitza-Dirac effect.
4. The Lorentz force of the electron quiver in the oscillating in electric field [$\delta\mathbf{p} \times \mathbf{B}$ in Eq. (83a) (non-relativistic), $\langle (\mathcal{G} + \mathcal{F}) \times \mathbf{B} \rangle$ in Eq. (94) (relativistic)] dominates in classical ponderomotive motion.

Here, we mention that the points 1 and 2 can be shown to be mathematically equivalent [12]. Regarding point 2, we further state that the development of investigation in this work assumes alignment of the photon polarizations along the e_3 axis.

B. Relativistic transverse electron momentum $p_3 \gg mc$ situation in Fig. 5(b)

For clearness, we also formulate the converse of the statements in section VIA:

1. The coupling to positive intermediate states [blue dash-dotted in Fig. 4] in the electron-light interaction of the Kapitza-Dirac effect dominates over the coupling to negative intermediate states [red dashed line in Fig. 4 and (37b)].
2. A virtual electron-position pair does *not* dominantly contribute to the scattering dynamics in Compton scattering [corresponding to $|e_1^- \rangle$ and $|e_1^-, \gamma_+ \gamma_- \rangle$ in Eq. (33)].
3. An extrapolation from small to big transverse electron momenta indicates that also the $\mathbf{p} \cdot \mathbf{A}$ term [U^{nd} in Eqs. (66)-(70)] contributes to the Kapitza-Dirac quantum dynamics.
4. An extrapolation from the non-relativistic limit indicates that also the deflection of the electron trajectory $\delta\mathbf{B}$ due to the Lorentz force is influencing the Lorentz force [$\mathbf{p} \times \delta\mathbf{B}$ in Eq. (83a) (non-relativistic), $\langle \mathcal{C} \times \mathbf{B} \rangle$ in Eq. (94) (relativistic)] and contributes to the quantum dynamics.

VII. CONCLUSIONS AND OUTLOOK

In this article we have demonstrated that quantum dynamics in standing light waves, especially in the two-photon Kapitza-Dirac effect can be dominantly mediated by virtual negative excitations in the context of a single-particle relativistic quantum description of spin 1/2 particles of the Dirac equation. While the relativistic quantum- and classical descriptions result in consistent diffraction amplitudes, with respect to the electron's transverse momentum dependency, non-relativistic dynamics deviates due to a lack of the relativistic gamma factor. Nevertheless, it is interesting that the dominant negative state coupling in time-dependent perturbation theory for the case of small transverse electron momenta ($p_3 \ll mc$) can be equivalently associated with coupling to a virtual electron-positron pair in a fully quantized system, in the context of Compton scattering. In this context, it would be interesting to explore the relation of the dynamics to the Feynman-Stückelberg interpretation [10]. Does it really mean, that the configuration in Fig. 5(a) is an implementation, in which we have realized an electron which dominantly moves to the future to scatter at the first photon then travels back in time to scatter with the second photon, for finally propagating further into the future? Another research question arises from the consideration that negative states with a certain canonical momentum are subject to the negative dispersion of their negative energy-momentum relation. This

negative energy-momentum relation causes an opposite motion as compared to their positive counterparts. The question arises: What happens, if one applies an electric field to the oppositely moving and oppositely charged negative states, and how this opposite motion influences the quantum dynamics of, for example the Kapitza-Dirac diffraction, and does it influence the process of virtual excitations to become real?

ACKNOWLEDGMENTS

The work was supported by the National Natural Science Foundation of China (Grant No. 12535015).

Appendix A: Nonrelativistic limit of Dirac equation

It is illustrative for the perception of negative state coupling to be aware about the derivation of the non-relativistic limit of the Dirac equation. The calculation about the non-relativistic limit can be found in standard text books on advanced quantum theory [1, 2, 10] and we follow the notion in references [2, 10] in the following. First, we introduce the abbreviation

$$\boldsymbol{\pi} = \mathbf{p} - \frac{e}{c} \mathbf{A}. \quad (\text{A1})$$

Inserting the two component approach

$$\Psi = \begin{pmatrix} \varphi \\ \chi \end{pmatrix} \exp \left(-\frac{imc^2}{\hbar} t \right) \quad (\text{A2})$$

with spinors φ and χ into the Dirac equation (3) and (4) yields

$$i\hbar \frac{\partial}{\partial t} \begin{pmatrix} \varphi \\ \chi \end{pmatrix} = c \begin{pmatrix} \boldsymbol{\sigma} \cdot \boldsymbol{\pi} \chi \\ \boldsymbol{\sigma} \cdot \boldsymbol{\pi} \varphi \end{pmatrix} - 2mc^2 \begin{pmatrix} 0 \\ \chi \end{pmatrix}. \quad (\text{A3})$$

Assuming that χ is a slowly varying function in time as compared to the electron rest mass oscillation in the complex plane, ie. $\partial\chi/\partial t \ll mc^2/\hbar$ allows for neglecting the time-derivative of χ . Within this approximation, the lower components in Eq. (A3) can be inverted for

$$\chi = \frac{\boldsymbol{\sigma} \cdot \boldsymbol{\pi}}{2mc} \varphi \quad (\text{A4})$$

and reinserted into the upper components, which yields

$$i\hbar \frac{\partial \varphi}{\partial t} = \frac{\boldsymbol{\pi}^2}{2m} \varphi + i \frac{\boldsymbol{\sigma}}{2m} \cdot \boldsymbol{\pi} \times \boldsymbol{\pi} \varphi. \quad (\text{A5})$$

Neglecting the spin term of the Pauli equation on the right of the right-hand side results in the Schrödinger equation with Hamiltonian (56). Note, that we only have arrived at the right-hand side because we inserted a coupling between the upper and lower components (A4) in the upper components in (A3). In other words: The wave function φ of the Schrödinger equation (or Pauli equation, respectively) at the upper component in Eq. (A3) had to be passed through the lower components of (A3), to become (A5).

We also point out that the approximate block-diagonalization of the Dirac equation in context of the Foldy-Wouthuysen transformations [1–3, 35] involves transitions to the negative spectrum as well. The term $\boldsymbol{\pi}^2$ in the Schrödinger equation arises from the squared appearance \mathcal{O}^2 of the block-off-diagonal term $\mathcal{O} = c\boldsymbol{\alpha} \cdot \boldsymbol{\pi}$, which is generating the Foldy-Wouthuysen transformation through the generator $S = -i\beta\mathcal{O}/2mc^2$. The off-diagonal structure of \mathcal{O} due to the off-diagonal alpha matrices $\boldsymbol{\alpha}$ implies the transition to negative states. This also holds for the relativistic correction of the kinetic energy term, which is proportional to \mathcal{O}^4 .

[1] A. Wachter, *Relativistic Quantum Mechanics* (Springer Netherlands, 2011).
[2] F. Schwabl, *Advanced Quantum Mechanics* (Springer, 2000).
[3] W. Greiner, *Relativistic Quantum Mechanics. Wave Equations* (Springer Berlin, Heidelberg, 2000).
[4] O. Klein, Quantentheorie und fünfdimensionale Relativitätstheorie, *Zeitschrift für Physik* **37**, 895–906 (1926).
[5] W. Gordon, Die Energieniveaus des Wasserstoffatoms nach der Diracschen Quantentheorie des Elektrons, *Zeitschrift für Physik* **48**, 11–14 (1928).
[6] P. A. M. Dirac, The quantum theory of the electron, *Proc. Roy. Soc. Lond. A* **117**, 610 (1928).
[7] P. A. M. Dirac, A theory of electrons and protons, *Proc. Roy. Soc. Lond. A* **126**, 360 (1930).
[8] C. D. Anderson, The Apparent Existence of Easily Deflectable Positives, *Science* **76**, 238 (1932).
[9] J. R. Walter Greiner, *Field Quantization* (Springer Berlin, Heidelberg, 1996).
[10] W. Greiner, B. Müller, and J. Rafelski, *Quantum Electrodynamics of Strong Fields* (Cambridge University Press, 1985).
[11] M. E. Peskin and D. V. Schroeder, *An Introduction to Quantum Field Theory* (Westview Press, 1995).
[12] S. Ahrens, Z. Liang, T. Čadež, and B. Shen, Spin-dependent two-photon Bragg scattering in the Kapitza-Dirac effect, *Phys. Rev. A* **102**, 033106 (2020).
[13] P. L. Kapitza and P. A. M. Dirac, The reflection of electrons from standing light waves, *Math. Proc. Cambridge Philos. Soc.* **29**, 297 (1933).

- [14] H. Batelaan, The Kapitza-Dirac effect, *Contemp. Phys.* **41**, 369 (2000).
- [15] H. Batelaan, *Colloquium* : Illuminating the Kapitza-Dirac effect with electron matter optics, *Rev. Mod. Phys.* **79**, 929 (2007).
- [16] S. Ahrens, H. Bauke, C. H. Keitel, and C. Müller, Spin Dynamics in the Kapitza-Dirac Effect, *Phys. Rev. Lett.* **109**, 043601 (2012).
- [17] S. Ahrens, H. Bauke, C. H. Keitel, and C. Müller, Kapitza-Dirac effect in the relativistic regime, *Phys. Rev. A* **88**, 012115 (2013).
- [18] S. Ahrens, Electron-spin filter and polarizer in a standing light wave, *Phys. Rev. A* **96**, 052132 (2017).
- [19] D. L. Freimund, K. Aflatooni, and H. Batelaan, Observation of the Kapitza-Dirac effect, *Nature (London)* **413**, 142 (2001).
- [20] D. L. Freimund and H. Batelaan, Bragg Scattering of Free Electrons Using the Kapitza-Dirac Effect, *Phys. Rev. Lett.* **89**, 283602 (2002).
- [21] S. Ahrens, *Investigation of the Kapitza-Dirac effect in the relativistic regime*, Ph.D. thesis, Ruprecht-Karls University Heidelberg (2012), <http://archiv.ub.uni-heidelberg.de/volltextserver/14049/>.
- [22] M. O. Scully and M. S. Zubairy, *Quantum Optics* (Cambridge University Press, 1997).
- [23] S. Ahrens, Z. Guan, and B. Shen, Beam focus and longitudinal polarization influence on spin dynamics in the Kapitza-Dirac effect, *Phys. Rev. A* **105**, 053123 (2022).
- [24] J. J. Sakurai and J. Napolitano, *Modern Quantum Mechanics*, 3rd ed. (Cambridge University Press, 2020).
- [25] F. Halzen and A. D. Martin, *Quarks and Leptons* (Wiley, 1984).
- [26] S. Weinberg, *The Quantum Theory of Fields*, Vol. I (Cambridge University Press, 1995).
- [27] O. Smirnova, D. L. Freimund, H. Batelaan, and M. Ivanov, Kapitza-dirac diffraction without standing waves: Diffraction without a grating?, *Phys. Rev. Lett.* **92**, 223601 (2004).
- [28] J. D. Jackson, *Classical Electrodynamics*, third edition ed. (Wiley, 1999).
- [29] D. Bauer, P. Mulser, and W. H. Steeb, Relativistic Ponderomotive Force, Uphill Acceleration, and Transition to Chaos, *Phys. Rev. Lett.* **75**, 4622 (1995).
- [30] A. E. Kaplan and A. L. Pokrovsky, Fully Relativistic Theory of the Ponderomotive Force in an Ultraintense Standing Wave, *Phys. Rev. Lett.* **95**, 053601 (2005).
- [31] A. L. Pokrovsky and A. E. Kaplan, Relativistic reversal of the ponderomotive force in a standing laser wave, *Phys. Rev. A* **72**, 043401 (2005).
- [32] P. W. Smorenburg, J. H. M. Kanters, A. Lassise, G. J. H. Brussaard, L. P. J. Kamp, and O. J. Luiten, Polarization-dependent ponderomotive gradient force in a standing wave, *Phys. Rev. A* **83**, 063810 (2011).
- [33] J. Ribbing, G. Perosa, and V. Goryashko, Relativistic ponderomotive force in the regime of extreme focusing, *Opt. Lett.* **50**, 2093 (2025).
- [34] See Supplemental Material at [url will be inserted by publisher] for the details of the derivation of the relativistic ponderomotive potential.
- [35] L. L. Foldy and S. A. Wouthuysen, On the Dirac Theory of Spin 1/2 Particles and Its Non-Relativistic Limit, *Phys. Rev.* **78**, 29 (1950).